ornl

OAK RIDGE NATIONAL LABORATORY

UNION CARBIDE

ORNL/TM-7219

Models for Impurity Effects in Tokamaks

J. T. Hogan

OPERATED BY
UNION CARBIDE CORPORATION
FOR THE UNITED STATES
DEPARTMENT OF ENERGY

Printed in the United States of America. Available from
National Technical Information Service
U.S. Department of Commerce
5285 Port Royal Road, Springfield, Virginia 22161
NTIS price codes—Printed Copy: A03; Microfiche A01

ORNL/TM-7219
Dist. Category UC-20 g

Contract No. W-7405-eng-26

FUSION ENERGY DIVISION

MODELS FOR IMPURITY EFFECTS IN TOKAMAKS

J. T. Hogan

Date Published - March 1980

Prepared by the
OAK RIDGE NATIONAL LABORATORY
Oak Ridge, Tennessee 37830
operated by
UNION CARBIDE CORPORATION
for the
DEPARTMENT OF ENERGY

CONTENTS

ABSTRACT

Models for impurity effects in tokamaks are described with an emphasis on the relationship between attainment of high β and impurity problems. We briefly describe the status of attempts to employ neutral beam heating to achieve high β in tokamaks and propose a qualitative model for the mechanism by which heavy metal impurities may be produced in the startup phase of the discharge. We then describe paradoxes in impurity diffusion theory and discuss possible resolutions in terms of the effects of large-scale islands and sawtooth oscillations. Finally, we examine the prospects for the Zakharov-Shafranov catastrophe (long time scale disintegration of FCT equilibria) in the context of present and near-term experimental capability.

1. INTRODUCTION

In the attempt to make the tokamak confinement system a more attractive economic performer at the reactor stage, two major lines of improvement are being followed.

The first of these is to boost the amount of nuclear power obtained from a given plasma volume. This increase in power density leads to a requirement for plasma β values exceeding the $\sim$1% values typical of tokamak experiments in the past.

The other improvement requires a lengthening of the duration of the discharge. Although steady state operation is optimum, most practical economic requirements can be met with a long (tens of seconds) but finite pulse length. Typical experimental pulse lengths never exceed 1 s, and even though they are in equilibrium with repsect to the energy and particle transport processes, the magnetic configuration and equilibration of the plasma and wall are still evolving.

It is the conflict between these two requirements, high power density (high β) and longer pulse length, that gives rise to the questions addressed here. Higher power density inevitably introduces concern about impurity generation. (If it did not, the power density would be increased to the point at which the incremental return, balanced against impurity losses, was small.) In turn, because the impurity content strongly influences the resistivity, the impurity effects on the magnetic configuration (shear, curvatures, etc.) will play a determining role in predicting the actual β limit in any reactor system.

Some issues in these areas are now being addressed by tokamak experiments:

1. The presently accepted theoretical limits to β are set by the appearance of ideal MHD ballooning-interchange modes. It is not known whether these values for $\beta_{critical}$ are optimistic, pessimistic, or irrelevant.

2. The impurity production mechanism is unknown. Paradoxically, while charge exchanged, recycling neutrals should cause an inevitable impurity production in the high-temperature regime. However, significant

contributions of metal impurities are found just after startup in many experiments, when the energy of charge exchange neutrals is low.

3. Neoclassical theory predicts a continued accumulation of impurities. Experiments show mixed results; all experiments in which impurities are deliberately introduced indicate migration to the center of the discharge. However, a stable and continuous buildup is not observed.

4. High-β equilibria can be achieved with rapid heating according to FCT theory. The persistence of these states on the resistive time scale has been questioned.

Some recent developments in these areas will be described here:

1. Experimental evidence for the validity of ideal MHD β limits, for circular geometry, has been obtained and can be tested against theoretical predictions.[1]

2. The initial phase of the tokamak discharge can be modelled more accurately so that the preheating magnetic configuration can be more reliably predicted and an important source of metallic impurities can be identified.

3. Important processes governing impurity transport can now be modelled. These are the effect of internal "sawtooth" relaxations in spreading the impurities and the screening effect of large-scale, saturated nonlinear tearing modes in resisting impurity accumulation.

4. Detailed data needs for more accurate modelling have been identified. These are low energy (10 eV-2 keV) cross sections for charge exchange reactions of the type $A^{n+} + H^{o} \rightarrow A^{(n-1)+} + H^{+}$ and low-dose, light-ion sputtering yields for interactions of charge exchange neutrals with wall/limiter surfaces.

5. The prospects for studying the maintenance of high-β (FCT) equilibria can be assessed more accurately.

2. TRANSPORT MODEL

The transport model we will use is described in Ref. 2. As shown in Fig. 1, we incorporate a description of ballooning stability developed by R. G. Bateman.[3] Results from this code, which is used as a module in the comprehensive transport code, have been presented in Ref. 4. (The future goal of modelling high-β experiments will be to close the loop shown in Fig. 1 by modifying transport rates with respect to ballooning stability/instability.) The Fokker-Planck fast ion model was developed by R. H. Fowler et al.,[5] and the 2-D Grad-Shafranov equation solver was formulated by D. C. Stevens.[6]

Except for the TOSCA cases, the calculations presented here use the empirical confinement scaling model:

$$\chi_e = \frac{5 \times 10^{17}\ \mathrm{cm^2\ s^{-1}}}{n_e} ,$$

$$D/\chi_e = \frac{1}{5} ,$$

and η, χ_i have three-regime neoclassical values.[2]

For TOSCA results, the Artsimovich pseudoclassical model was used for χ_e instead.[7]

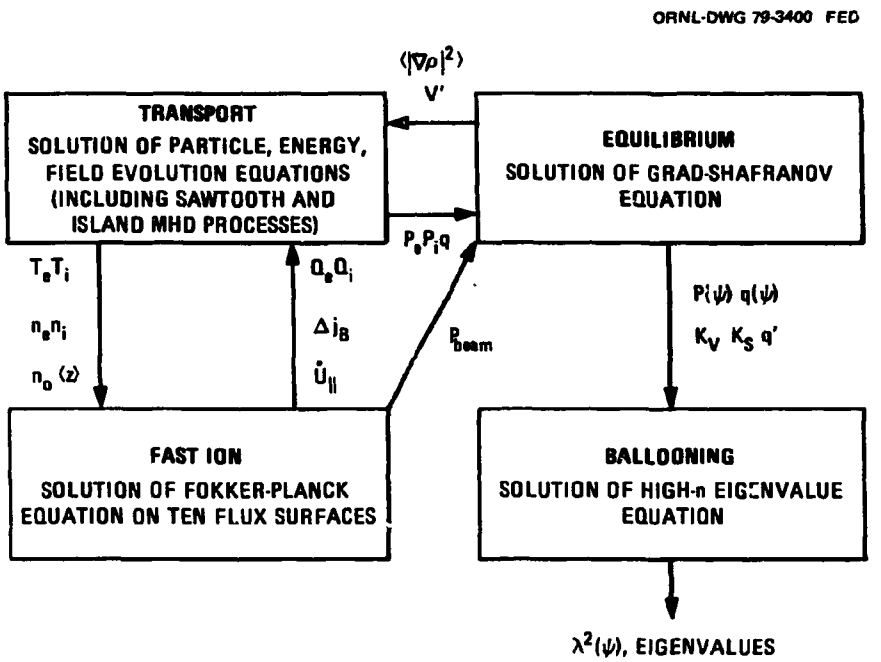

Fig. 1. Models used in ballooning-transport calculation. The radial Fokker-Planck transport processes (conduction, convection, beam heating, charge exchange, radiation) provide the pressure and shear profile for the 2-D equilibrium. The equilibrium variables determine the state of ballooning stability. When significant ballooning effects are discovered it may be possible to close the loop and to modify transport rates in regions of ballooning instability.

3. LOW-β, SHORT PULSE EFFECTS

Although the irreducible long pulse, high power density impurity problems are the major concern, important effects can develop in special situations at low β with short pulse length. As shown in Ref. 8, the adiabatic compression process[9] can be used to produce high neutron fluxes in D-T tokamaks. This technique will be used in TFTR, JET, and ignitor devices,[10-12] with ignition being the goal of the latter.

However, radiative losses are

$$P_{rad} = n_e n_z f(T_e) .$$

The density scales as C^2 (C is the compression factor $\equiv R_{initial}/R_{final}$; R is the major radius). Thus, with compression,

$$P_{rad} \sim C^4 .$$

Hence, if heavy metal impurities (M_o, W) are used, the injection/compression process decreases the possibility of ignition.[2]

4. HIGH-β, SHORT PULSE EFFECTS

Present tokamak experiments have produced β values in the regime $\beta \sim \beta_{critical}$. The β limit for reactors is set by criteria derived for the onset of ballooning interchange modes, which occur at high pressure.

Two sets of criteria should be distinguished. The first, derived from minimization of δW by large-scale, multidimensional codes, shows that modes with low toroidal wave number ($n \sim 1,3$) are the most dangerous. These modes have a structure that extends throughout the plasma volume.[13] Parametric studies of the criteria derived from the codes have been published.[14]

A second approach to the ballooning problem has been to use a high-n number expansion (that is, high toroidal mode number). With this approximation, the calculation is simplified and the β limit turns out to be very close to that predicted by the δW codes.[15] Moreover, in the high-n case, the stability criterion for balloning reduces to an ordinary differential equation along a field line. It is feasible to incorporate such a calculation with the other models in a transport code.

A typical calculated evolution sequence for ISX-B conditions is shown in Figs. 2-4. The pressure profile is quite peaked, with $\partial P/\partial\psi$ large near the magnetic axis. Thus, the ballooning eigenmode evolution shows that the stability criterion is violated over a substantial portion of the plasma.

PEST code results lead to a similar conclusion. The comparison in Fig. 5 of ISX-B β^* values with the $\beta^*_{critical}$ published in Ref. 14 shows that $\beta^* > \beta^*_{critical}$ has been achieved. The following should be noted:

1. The experimental cross section for these cases, although forced to be circular by external vacuum shaping fields, could have significant local deviations form noncircularity. This is especially true of cases in which beam penetration is good, leading to a strong central $B \times \nabla P/B^2$ current. By comparison, the vacuum field coils must act at a relatively great distance; thus, the local current has a stronger effect. With elongation, $\beta_{critical}$ rises; therefore, local changes in cross section could stabilize the mode.

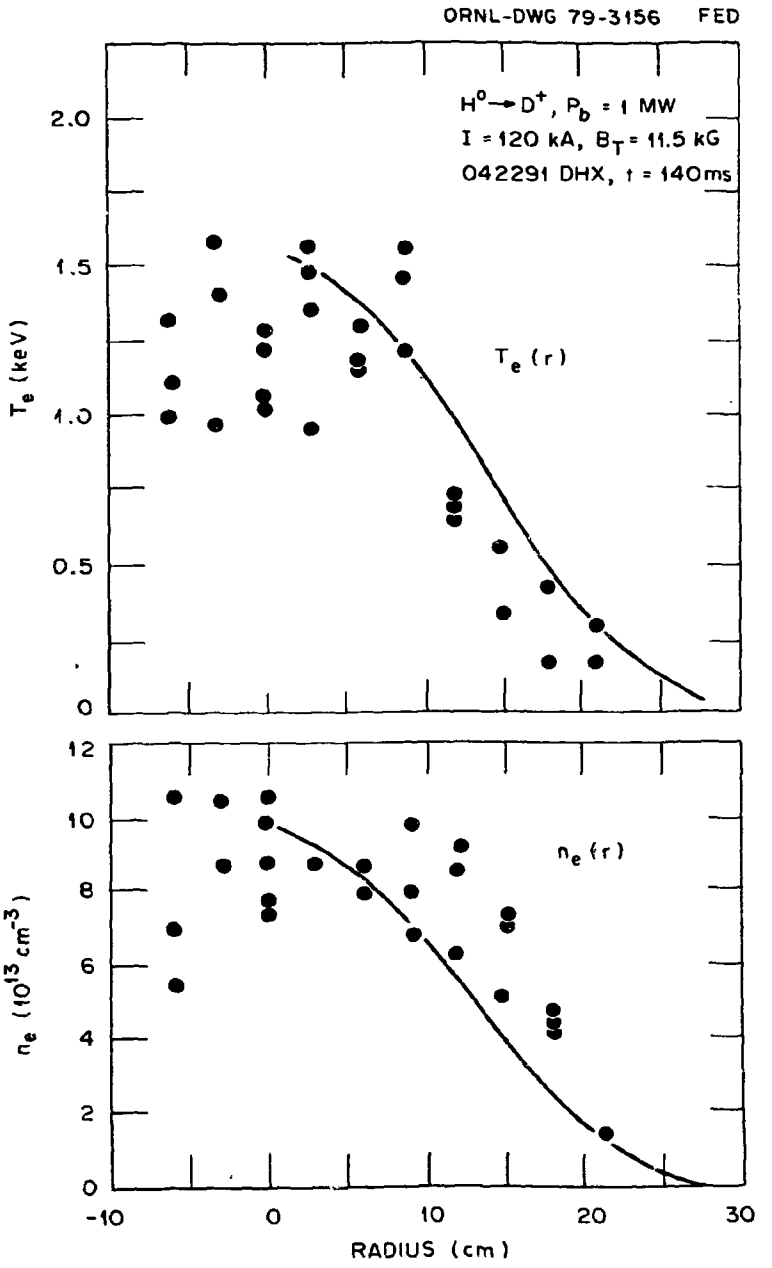

Fig. 2. Thomson scattering results for electron temperature and density profiles in an ISX-B 1-MW heating case. Although Alcator scaling and iron radiation combine to produce satisfactory agreement of code profiles with the data, the aim is simply to reproduce the thermal pressure profile for use in equilibrium and stability calculations.

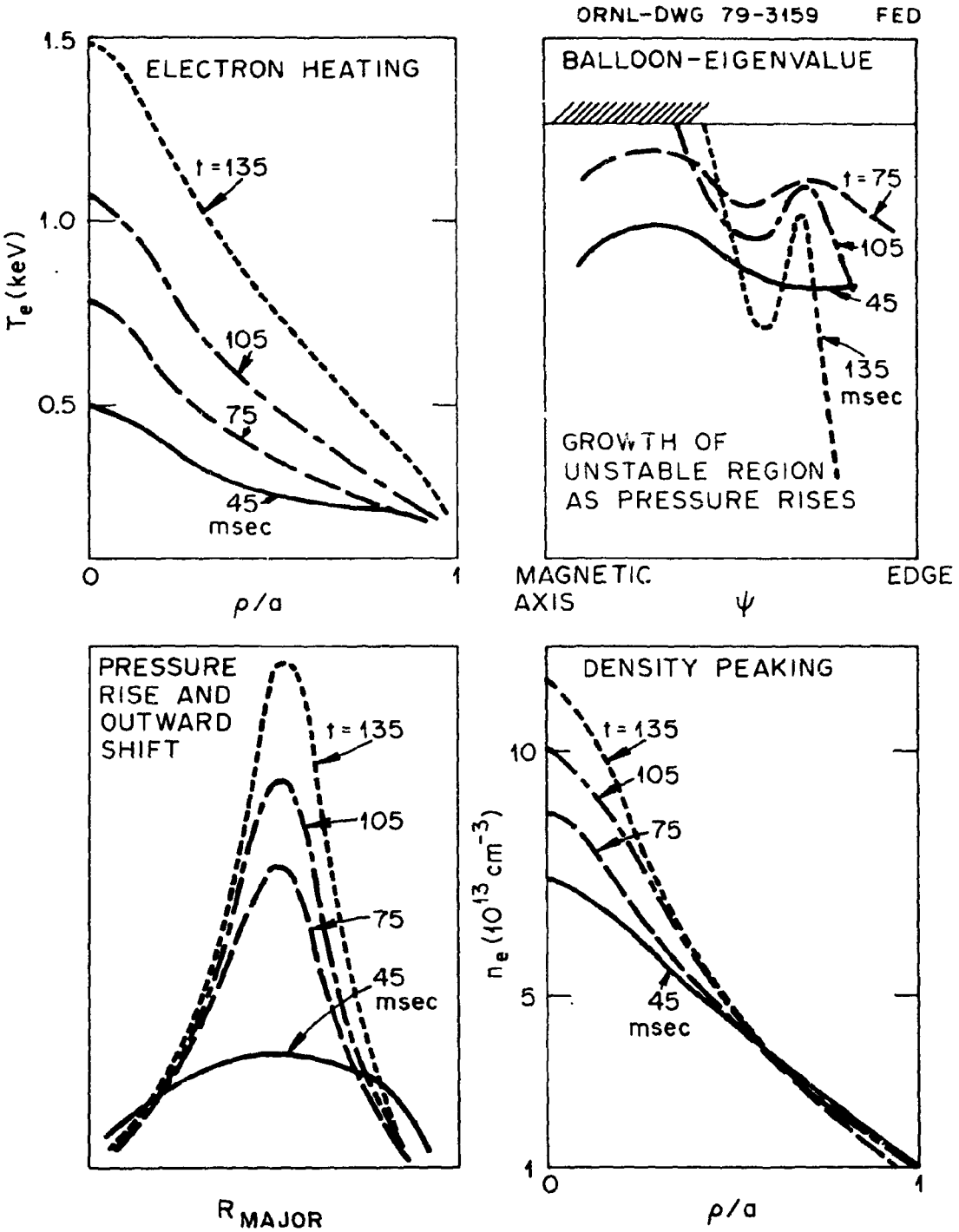

Fig. 3. Computer parameter evolution during ISX-B neutral beam heating (case shown in Fig. 2). The strong central peaking in pressure leads to a central zone of predicted ballooning instability (shaded region). The eigenvalues d evolve from completely negative (stable) to mixed values as p′ increases near the center.

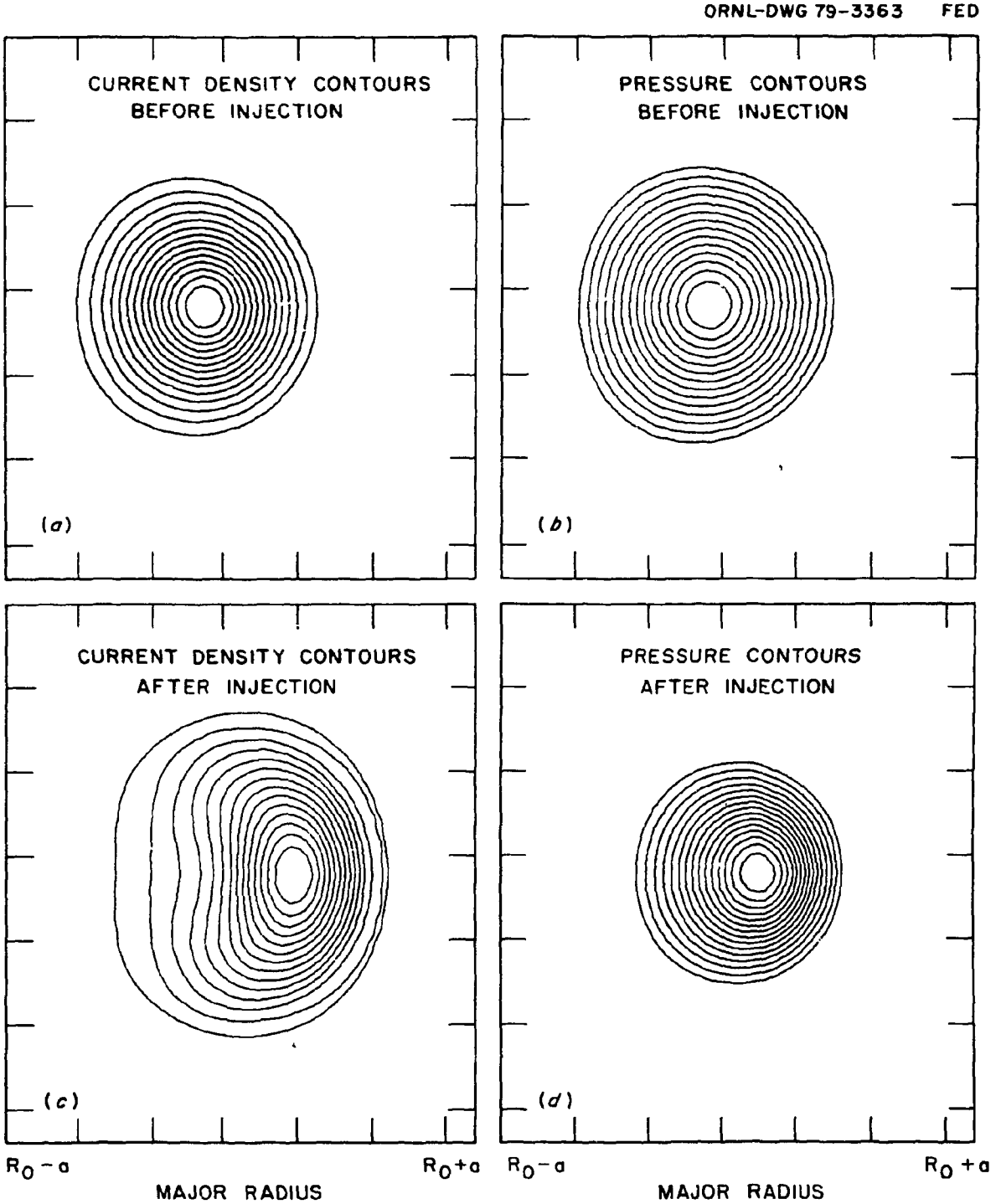

Fig. 4. The pressure and current density level contours before and after injection for the case described in Figs. 2-3. Although the pressure profiles are circular before and after injection, the strong $BXVP/B^2$ contribution to the local current density at high β produces strongly distorted, noncircular current density profiles.

2. The theoretical results in Fig. 5 assume $P = P(\psi - \psi_o)^2$. For more peaked profiles, the $\beta_{critical}$ drops, counteracting the rise in $\beta_{critical}$ that results from possible elongation. The combined result (cross section change vs peaking) is to restore the β limit in Fig. 5 to its original place, i.e., $\beta^*_{exp} > \beta^*_{critical}$.

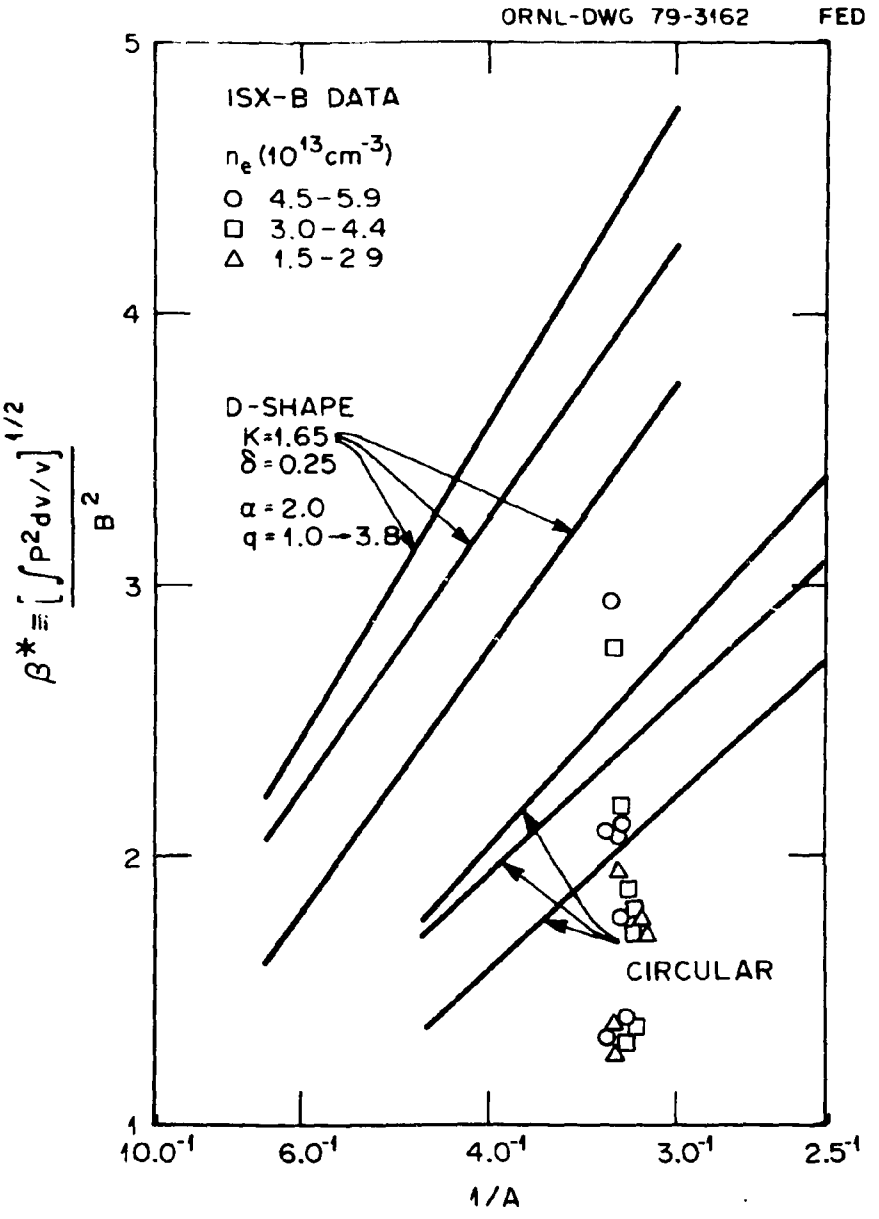

Fig. 5. Comparison of measured ISX-B β* values with predicted critical β* for circular plasma from the PEST code. Because possible noncircularity and pressure profile peaking are opposing, these values indicate the $\beta^* > \beta^*_{critical}$ for these cases.

5. IMPURITY EFFECTS

Recent developments in several areas relate to long pulse, high-β tokamak improvements.

5.1 INITIAL PHASE: IMPURITY PRODUCTION

A major flaw in tokamak transport codes in the past has been the lack of a uniformly valid model for dealing with the current penetration in large machines. Scenarios for avoiding a disastrous skin effect have been proposed. However, there has been no real reason to expect such a problem because similar results were predicted but not observed on smaller experiments. If transport models reproducing the steady state phase parameters are used in the initial phase, the results are as shown in Fig. 6. A large skin current results, in contrast to the lack of such a current in experiments.

Recent computational and experimental developments have yielded a serviceable model for startup to be used in transport codes. Work on the detailed structure of the model is still needed, but the picture is sufficiently clear to enable us to replace the deficient model shown in Fig. 6 with one more faithful to reality. Moreover, this model has some important implications for the mechanism of impurity production.

On the experimental side, detailed probe measurements during the initial phase by Mirnov and Semenov[16] have disclosed a regular series of MHD disruptions with progressively decreasing mode numbers. These authors refer to the linear MHD theory of Shafranov[17] to interpret these results and cite a repetitive process of the formation of a weak skin current followed by MHD relaxation.

Detailed computational work using a 2-D code to describe the nonlinear evolution of resistive tearing modes has given a more accurate theoretical model.[18] In this model the criterion for reconnection is

$$\psi^*(0) \cong \psi^*(\bar{r}_s) \ .$$

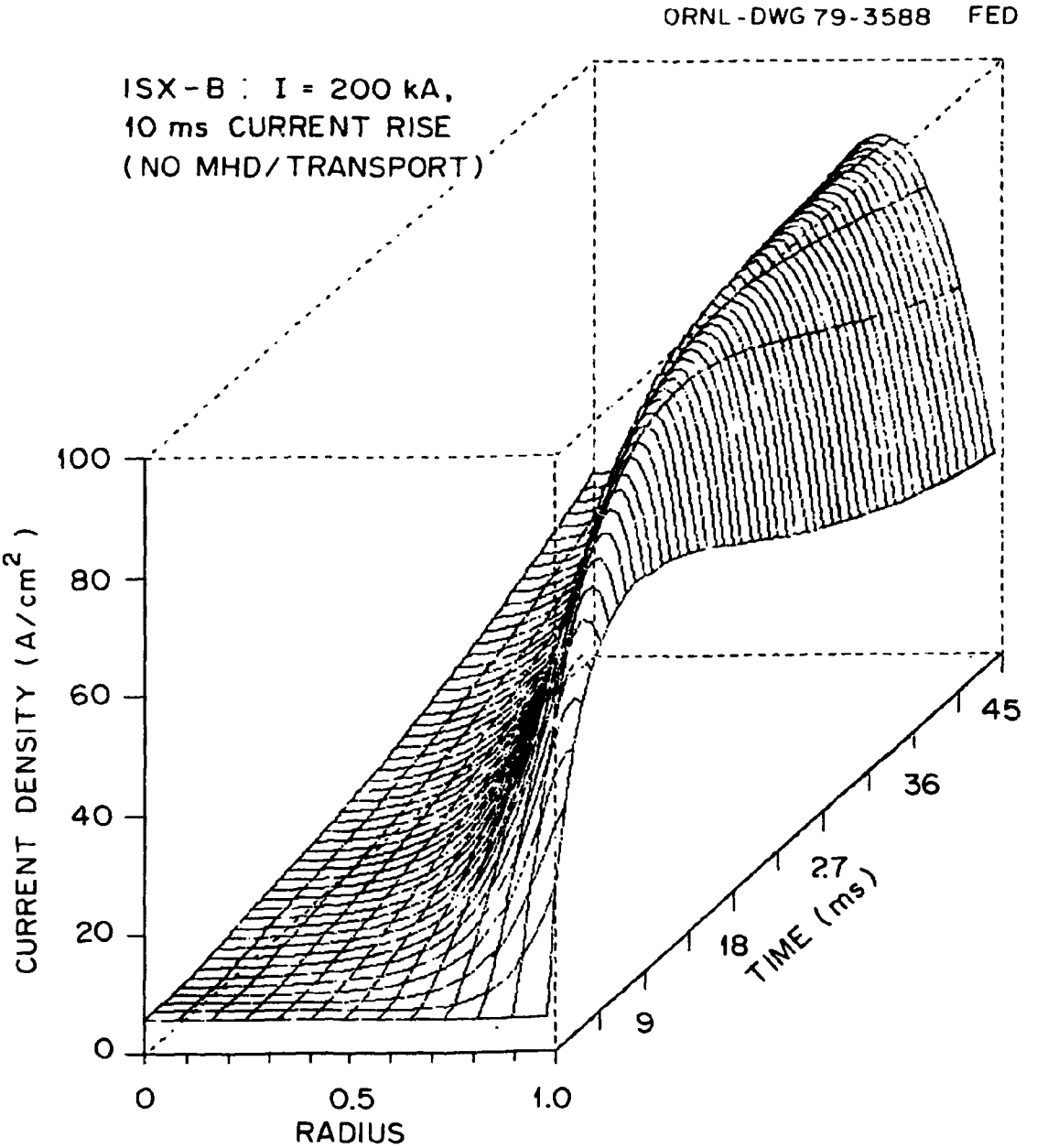

Fig. 6. Current penetration calculated for ISX-B without the MHD relaxation model. The attempt to produce a 200-kA current in 25 ms leads to a pronounced edge peaking of the current, unlike that of the experimental observation.

Here, the helical flux $\psi^*(r)$ is defined by

$$-\frac{d\psi^*}{dr} = B^* = B_{pol}\left|1 - \frac{n}{m}\, q(r)\right|, \qquad (1)$$

where B_{pol} is the poloidal magnetic field; m and n are the poloidal and toroidal mode numbers, respectively; and q(r) is the local Kruskal-Shafranov safety factor. If r_{s_1} and r_{s_2} are the two spatial locations at which $q(r_{s_1}) = m/n$ with a nonmonotone profile, then $\bar{r}_s = 1/2(r_{s_1} + r_{s_2})$. Thus, the reconnection criterion can be easily applied in transport calculations by following the poloidal field evolution and mixing the plasma parameters over the region internal to $\bar{r}_s$ at the time of reconnection. Extensive transport calculations along these lines have been performed by Dnestrovskii and coworkers.[19]

The resulting evolution in this model, for the same case as in Fig. 6, is shown in Fig. 7. We see a series of small relaxations that produce a smooth rise in the current. We should note that a typical change in specific internal inductance, as shown in Fig. 7, is $\Delta\ell \cong 0.07$.

Impurity production by arcing is an actively researched area at present. Although quantitative criteria can be given for the number of micrograms of material removed per Coulomb of charge passed in an established arc, it is not possible to give a quantitative estimate for the probability of an arc strike. Nevertheless, the MHD model allows a qualitative conclusion.

The reconnection process produces a small disruption with a plasma shift. The direction of the shift depends on which of the terms in $\beta_{pol} + \ell_i/2$ is the larger.[20] Each shift results in the contact of the wall and the plasma with a few hundred electron volts of electron temperature establishing a sheath and likely inducing arcing activity. Such activity has been observed by Miodezcewski et al. on ISX-A.[21]

This arcing process produces both light and heavy impurities. As seen in Fig. 8a, the T4 tokamak has been used to establish the mode structure of the startup relaxation oscillations. In an independent spectroscopic study, Scheglov[22] has observed an enhanced influx of carbon atoms during periods of MHD rearrangement (Fig. 8b).

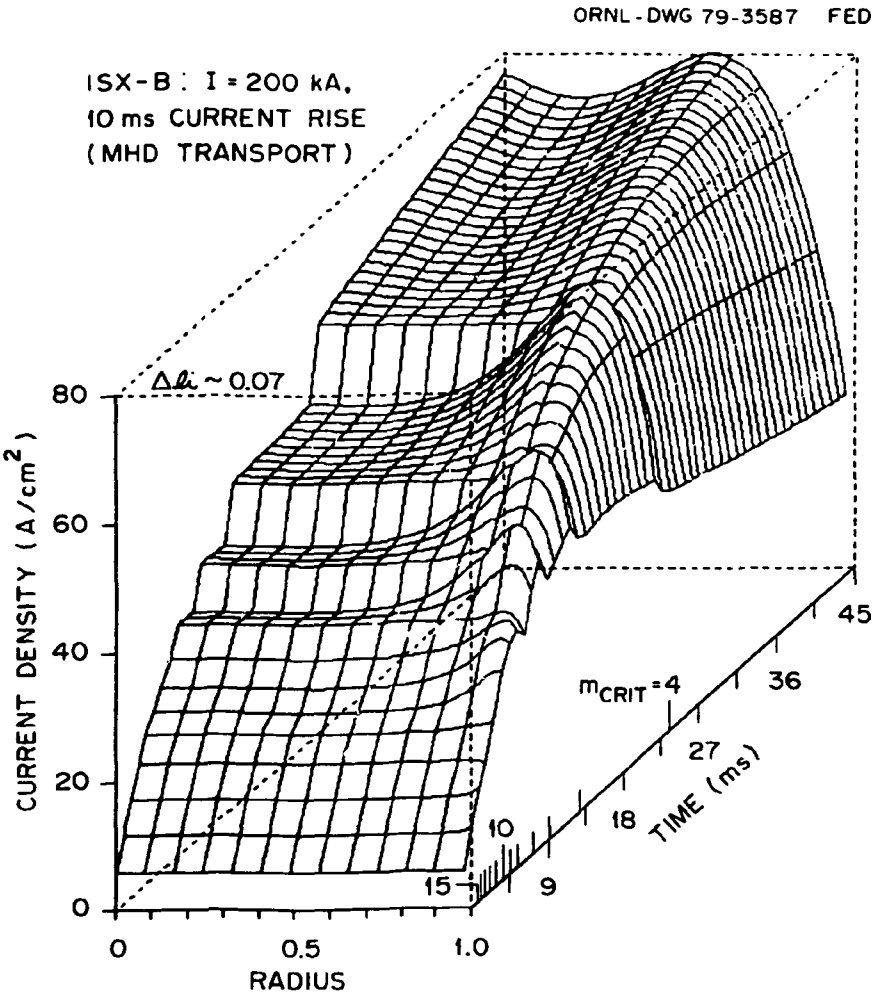

Fig. 7. Current penetration for the case of Fig. 6 with the MHD reconnection model. The periodic redistribution of flow gives an associated plasma shift (proportional to $\Delta \ell i$). This shift leads to the enhanced probability of arcing, with the high T_e plasma contacting the wall or limiter.

ORNL-DWG 79-3584 FED

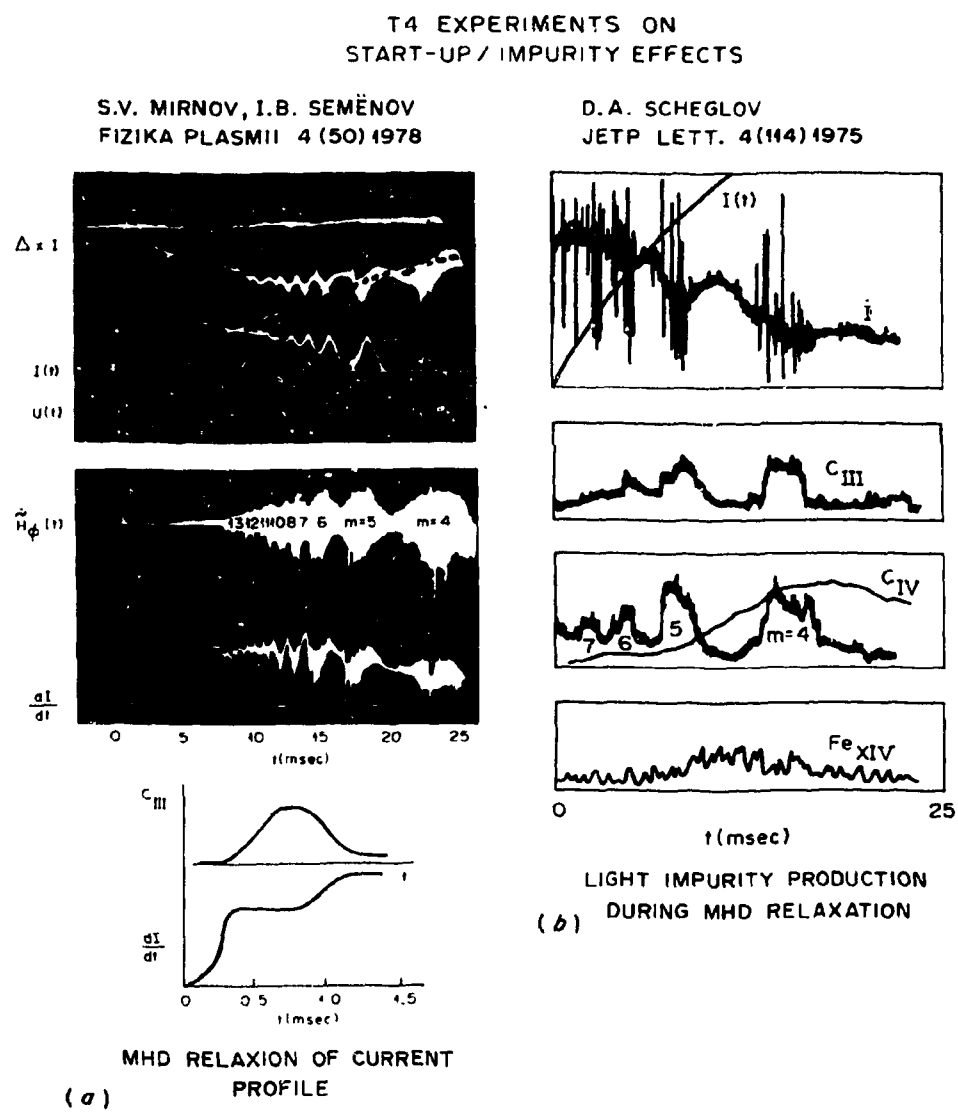

Fig. 8. (a) Results from MHD probes for a T4 discharge showing the periodic reconnection processes from modes with m = 14 and lower. (b) Corroborative spectroscopic information, also from T4, showing the correlation of impurity production with MHD activity.

5.2 "SAWTOOTH" MODES AND EFFECTS ON IMPURITY TRANSPORT

Kadomtsev[23] has proposed a model for the internal disruption prevalent in high current discharges. Similar to the startup reconnection model described in Sect. 5.1 (and actually antedating it), the helical flux is redistributed periodically, as are the plasma density and temperature. This MHD time scale model allows better agreement between impurity transport calculations using the neoclassical model and experiments that have been carried out to test this theory.

On the T4 tokamak, small amounts of argon were injected deliberately to measure the inward diffusion rate and to see whether continued accumulation would occur.[24,25] It was first noted that Ar^{15+} ions began to radiate from the core of the discharge sooner than neoclassical calculations predicted they should. Though not stated in Ref. 24, it is known that sawtooth oscillations were present in these discharges,[25] with the singular surface radius $r_{q=1} \cong 3$ cm. Thus, the radius within which mixing occurs, r_o, is a large fraction of the minor radius a: a = 17 cm, $r_o \cong 5$ cm [r_o is defined by the condition $\psi^*(0) = \psi^*(r_o)$].

Figure 9 shows the effect on the interpretation of the initial rise of argon density in the core. Without sawtooth mixing there is a 10-15 ms delay before a substantial argon density rise is seen. With such a mixing process, $\tau_{rise} \cong$ 5-10 ms, in agreement with the experimental results. These calculations employ a relatively simple, yet reasonably accurate model for impurity transport. We solve

$$\frac{\partial n_z}{\partial t} = \frac{1}{r}\frac{\partial}{\partial r} rD \frac{\partial n_z}{\partial r} - rC_{zp}\left[\langle z\rangle n_z\left(\frac{\partial n_p}{\partial r} + \alpha_1 n_p \frac{\partial \ell n\, T_p}{\partial r}\right)\right.$$

$$\left. - n_p\left(\frac{\partial n_z}{\partial r} + \alpha_z n_z \frac{\partial \ell n\, T_p}{\partial r}\right)\right] + rC_{zz}\left[(\langle z^2\rangle - \langle z\rangle^2)n_z\right.$$

$$\left. \cdot\left(\frac{\partial n_z}{\partial r} + \alpha_z n_z \frac{\partial \ell n\, T_p}{\partial r}\right) - \langle z\rangle n_z^2 \frac{\partial\langle z\rangle}{\partial r}\right], \quad (2)$$

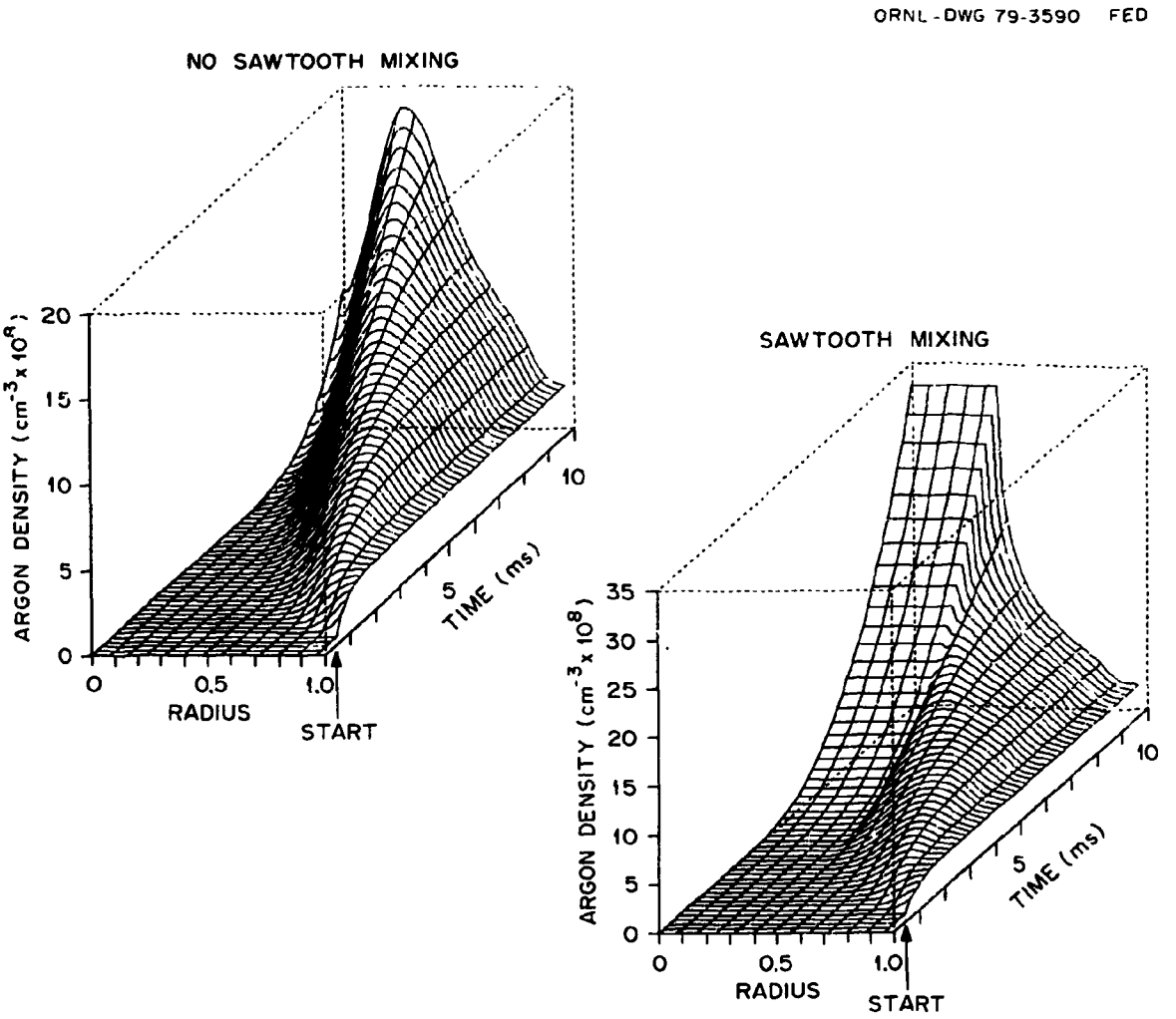

Fig. 9. Argon injection with/without sawtooth mixing. The uniform mixing of plasma parameters over the central zone leads to a quicker rise in the observed central radiation.

where D is the particle diffusivity and C_{zp}, C_{zz}, and α_1/α_2 are defined in Ref. 10. The boundary conditions are that a flux of neutral argon atoms is prescribed at r = a.

This "average ion" model is complemented by coronal equilibrium expressions for <z> taken from data tables published by D. E. Post et al.[26]

The sawtooth spreading alone cannot account for the saturation of core impurity density observed in the T4 experiments; thus, we must look for another mechanism.

5.3 EFFECTS OF LARGE-SCALE MAGNETIC ISLANDS

The nonlinear resistive tearing codes referred to earlier have also produced criteria for the nonlinear saturation of linearly unstable modes with $m \geq 2$, $n = 1, 2$. These saturated states, the Friedrichs "pinch buckling" equilibria,[27] have a helical structure imbedded in an otherwise axisymmetric geometry. Having a large radial extent centered at the singular surface $r = r_s$ [$q(r_s) = m/n$], they produce magnetic islands with width $W/a \lesssim 0.2$. Transport estimates[28] show a large enhancement of the diffusion rate across the island.

The island width calculation is relatively straightforward.[29] We compute the linear eigenmode from the ordinary differential equation (for m = 2, n = 1):

$$\frac{1}{r}\frac{d}{dr}\left(r\frac{d\psi_{21}}{dr}\right) - \frac{4}{r^2}\psi_{21} = \frac{2}{r}\frac{dJ_z^o}{dr}\frac{1}{F_{21}}\psi_{21} \qquad (3)$$

and

$$F_{21} = 1 - \frac{2}{q}J_z^o: \quad \text{equilibrium current density.}$$

Employing the criterion derived by White et al.,[30]

$$\Delta'(W) = 0 \ ,$$

we find the island width centered about $r = r_2$, $[q(r_2) = 2]$.

This transport enhancement has a large effect on the predictions of neoclassical theory concerning the accumulation of impurities. Because electrons follow the field lines more closely, they suffer a larger enhancement in radial diffusion than the ions. Thus, there is a significant enhancement of the relative electron and ion anomalous diffusion rates. If we follow the notation of Stringer[31] and denote the difference between electron and ion anomalous diffusion rates due to island effects as Γ_b, then the electron flux is given by:

$$\Gamma_e = \Gamma_{e_N} - D \frac{\partial n_e}{\partial r} + \Gamma_b \ , \tag{4}$$

where Γ_{e_N} is the pure neoclassical electron flux, which can be neglected in comparison with $D(\partial n_e/\partial r)$. The ambipolarity condition

$$\Gamma_e = \Gamma_p + \sum_k z_k \Gamma_k \tag{5}$$

requires a radial electrostatic field to hold the proton diffusion down to the electron rate. Concurrently, it creates a $Zd\phi/dr$ electrostatic field for impurity ions, impelling them inward. With an island present and Γ_b large, the radial electric field is, after Stringer,

$$E_r = \eta^{-1} \frac{T_p}{z_e} \left[\frac{n_z'}{n_z} - \gamma_z \frac{T_p'}{T_p} + \frac{n_p}{n_z} \frac{m_p}{m_z} \frac{z\mu_z}{\mu_p} \left(\frac{n_p'}{n_p} - \gamma_1 \frac{T_p'}{T_p} \right) \right]$$

$$+ 0.685 \ \eta^{-1} \frac{eB_\theta^2}{r/R \ n_z m_z \mu_z} \gamma_b \ , \tag{6}$$

where $\eta = 1 + (n_p m_p \mu_p / n_z m_z \mu_z)$ and γ_z, μ_p, μ_z are defined in Ref. 31.

Thus, Γ_b can have a strong local effect in stopping the principal impurity impulsion mechanism, with the impurity flux

$$\Gamma_z = -\frac{n_z m_z \mu_z}{(n_p m_p \mu_p + n_z m_z \mu_z)} 1.46 \frac{r}{p} \frac{n_p m_p \mu_p T_p}{z^2 e^2 B_\theta^2} \frac{n_z'}{n_z} - \gamma_2 \frac{T_p'}{T_p}$$

$$- z\left(\frac{n_p'}{n_p} - \gamma_1 \frac{T_p'}{T_p}\right) - \frac{\Gamma_b}{Z} - D \frac{\partial n_z}{\partial r} . \quad (7)$$

The strong relative flux of electrons with respect to protons at the magnetic island Γ_b produces an outward diffusion that can counteract the inward diffusion.

An example is shown in an ISX-B calculation in Fig. 10. The rise in ion temperature produced by neutral beam heating produces an iron influx in the calculation. This influx is determined by using available sputtering rates. (These are obtained with the weight-loss method. Because this method produces a substantial change in the surface state, it does not well reproduce the low-dose conditions of neutral beam heating experiments.) The impurities produced are held up at the location of the magnetic island. The inward diffusion rate is slowed, and Γ_z becomes positive (i.e., outward pointing) because an inverted n_z profile is built up.

Note that in contrast to earlier discussions of the effects of anomalous transport,[10,31] it is not the $D(\partial n_z/\partial r)$ term in Eq. (7) that produces the effect, but Γ_b — the difference in electron and proton diffusion caused by the large-scale island.

5.4 HIGH-β, LONG PULSE QUESTIONS

If the accumulation problem can be resolved by more detailed experiments with the help of the models described in the preceding sections, we will be faced with another problem unique to high-β, long pulse operation.

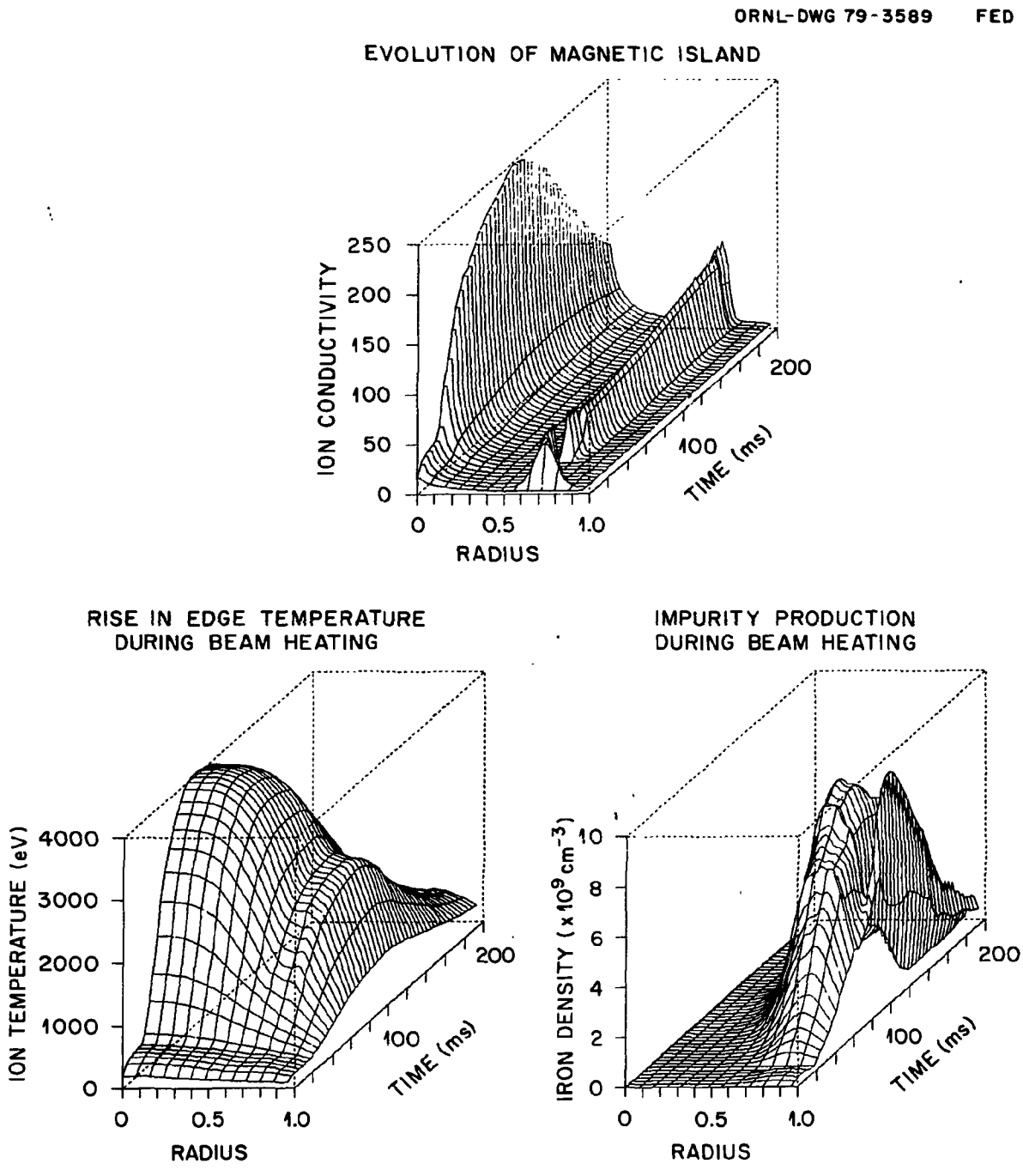

Fig. 10. The relationship between edge temperature, impurity production, impurity diffusion, and magnetic islands in an ISX-B neutral beam heating case. The rise in T_i edge due to heating leads to an increase in sputtered iron influx. The presence of a broad m = 2 island retards the inward impurity flow.

Zakharov and Shafranov have recently made the conjecture[32] that high-β equilibria cannot be maintained on a long time scale. They assert that states with $\beta_p > R/a$ can be achieved with rapid heating, which freezes the magnetic configuration. However, their calculations indicate that resistive diffusion will produce a separatrix, a null in the poloidal field, and an equilibrium instability in which sufficient plasma will be lost to the wall or divertor that $\beta_{pol} \leq R/a$. Zakharov and Shafranov have fixed the total plasma current during this resistive phase. Some objections have been raised to this assumption, however, because it has been shown that FCT equilibria can be retained by raising the current.[33] However, raising the current has the effect of lowering β_{pol} directly without requiring the instability. Similar remarks apply to expansion of the plasma volume as a remedy. Hence, one might expect that the search for FCT-preserving scenarios will occupy a good deal of attention in coming years.

To put this question in its present context, we show in Fig. 11 an ISX-B case extended to the present limits of beam technology (τ_{pulse} = 1.5 s). The plasma parameters equilibrate quickly, but the field evolution proceeds as iron atoms are sputtered in. The poloidal field on the inside tends toward zero during the rapid heating phase but then fills in as the temperature is decreased. Higher beam power and longer pulse length could provide an experimental test of this theoretical problem.

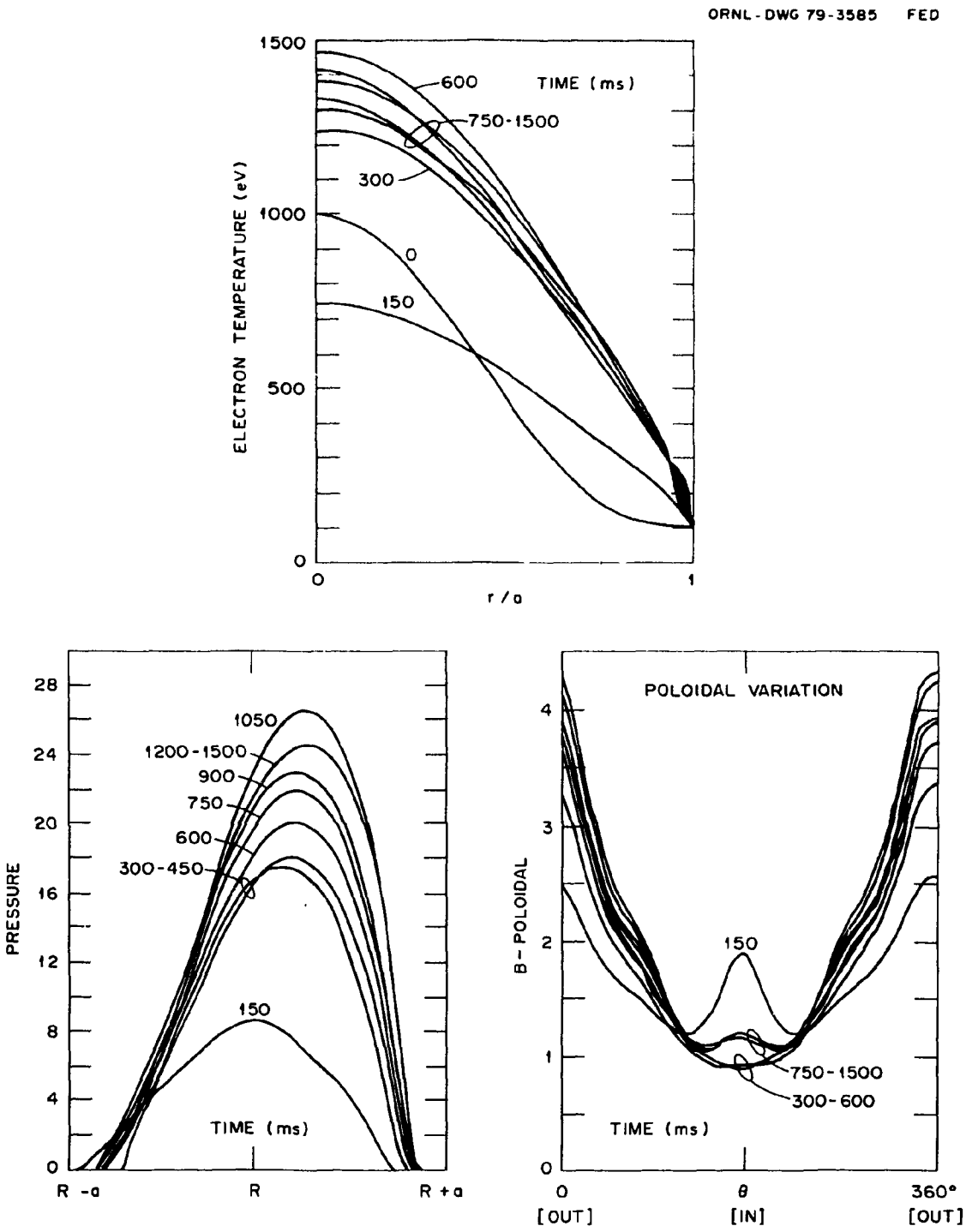

Fig. 11. Evolution of the ISX-B case considered earlier (Figs. 2-4) for 1.5 s. The poloidal field on the inside of the torus drops toward zero but reverses as impurities enter and β_{pol} decreases.

6. SUMMARY

The dual problems of increasing the power density and lengthening the pulse time of tokamak experiments lead to a number of plasma physics issues. Some progress has been recorded in these areas:

1. Comparison of ideal MHD theory with recent beam heating experiments shows that $\beta^* > \beta^*_{critical}$ has been achieved. A strong effect of local pressure-driven currents in the core flux surface shape can make a qualitative difference in ideal MHD predictions in well penetrated discharges.

2. Low-β, short pulse injection/compression schemes, such as those planned for JET, TFTR, Zephyr, and Ignitor(s), can worsen rather than improve the chances for ignition if heavy metal limiter/armor plate materials are used.

3. The initial phase (current penetration) in the tokamak discharge can be modelled without skin effect or significant anomaly. A qualitative model is proposed for the observed production of metallic impurities during this stage: arcing induced by the periodic MHD relaxations produces a strong electrostatic sheath, and ions accelerated by the sheath sputter the impurities.

4. The impurity accumulation paradox can be resolved by a combination of sawtooth mixing in the central core and large-scale MHD island effects. The island causes relative electron-proton enhanced diffusion and thus serves as a barrier to inward diffusion.

5. Long pulse evolution from FCT high-β states can be studied experimentally with beam pulse lengths of $\sim$1.5 s, the present technological limit.

REFERENCES

1. D. W. Swain et al., Controlled Fusion and Plasma Physics (Proc. 7th European Conf., Oxford, 1979), to be published.
2. J. Hogan, Nucl. Fusion 19, 753 (1979).
3. R. G. Bateman (Georgia Institute of Technology), private communication, 1979.
4. R. G. Bateman and D. B. Nelson, Phys. Rev. Lett. 41, 1804 (1978).
5. R. H. Fowler, J. Smith, and J. A. Rome, Comput. Phys. Commun. 13, 323 (1977).
6. D. C. Stevens (Courant Institute of Mathematical Sciences), private communication, 1975.
7. L. A. Artsimovich, Nucl. Fusion 12, 215 (1972).
8. H. P. Furth and D. L. Jassby, Phys. Rev. Lett. 32, 1176 (1974).
9. H. P. Furth and S. Yoshikawa, Phys. Fluids 13, 2593 (1970).
10. P. Rutherford, D. Düchs, and D. Post, Nucl. Fusion 17, 565 (1977).
11. JET Group, Commission of the European Communities Report EVR 579/e (EUR-JET-R8), Kirchberg, Luxembourg.
12. B. Coppi, Comments Plasma Phys. Controlled Fusion 3, 47 (1977).
13. R. G. Bateman and Y-K. M. Peng, Phys. Rev. Lett. 38, 829 (1977); A. M. M. Todd et al., Phys. Rev. Lett. 38, 826 (1977).
14. A. M. M. Todd et al., Nucl. Fusion 19, 743 (1979).
15. D. Dobrott et al., Phys. Rev. Lett. 39, 943 (1977); J. W. Connor, R. J. Hastie, and J. B. Taylor, Phys. Rev. Lett. 40, 396 (1978).
16. S. V. Mirnov and I. B. Semenov, Fiz. Plazmy 4, 50 (1978).
17. V. D. Shafranov, Sov. Phys.-Tech. Phys. 40, 241 (1970).
18. B. C. Carreras (Institute for Advanced Studies), private communication, 1979.
19. Y. N. Dnestrovskii et al., Fiz. Plazmy 5, 519 (1979).
20. R. S. Granetz, I. H. Hutchinson, and D. O. Overskei, Massachusetts Institute of Technology Report PFC/RR-79-14, Cambridge, Massachusetts (1979).
21. P. Miodezcewski, Proc. Plasma Materials Interactions Conf., Miami, 1979 (to be published).
22. D. A. Scheglov, JETP Lett. 4, 114 (1975).

23. B. B. Kadomtsev, Fiz. Plazmy 1, 710 (1975).
24. V. A. Abramov et al., Controlled Fusion and Plasma Physics (Proc. 8th European Conf., Prague, 1977), 1, 30 (1977).
25. V. A. Vershkov et al., Bull. Am. Phys. Soc. 23, 771 (1978).
26. D. E. Post et al., At. Data and Nucl. Data Tables (November 1977).
27. K. O. Friedrichs, Rev. Mod. Phys. 32, 889 (1960).
28. V. N. Pyatov and A. A. Shishkin, Nucl. Fusion 19, 831 (1979).
29. B. C. Carreras (Institute for Advanced Studies) and H. R. Hicks (Oak Ridge National Laboratory), private communication, 1979.
30. R. White et al., Phys. Rev. Lett. 39, 1618 (1977).
31. T. E. Stringer, *Lectures on Plasmas Near Breakeven* (Varenna, 1977), Pergamon Press, New York (1977).
32. L. E. Zakharov and V. D. Shafranov, Kurchatov Institute Report IAE 3075, Moscow, U.S.S.R. (1978).
33. D. B. Nelson, Lectures at the 1979 Varenna Conference on Plasmas Near Thermonuclear Conditions, Pergamon Press, New York (to be published).